Advanced Composite Materials
Publication details, including instructions for authors and subscription information:
http://www.tandfonline.com/loi/tacm20

Long-term durability of tri-axial woven CFRP tube structure extended along the spin axis of spinning platforms for the SCOPE mission

Jun Koyanagi[a], Akihito Watanabe[b], Nobuyoshi Kawabata[b], Tsuyoshi Ozaki[c], Ken Higuchi[d], Kosei Ishimura[e] & Yasumasa Kasaba[f]

[a] Department of Materials Science and Technology, Tokyo University of Science, Tokyo, Japan.

[b] Sakase Adtech Co. Ltd., Fukui, Japan.

[c] Composites Research and Development, Co. Ltd., Yokohama, Japan.

[d] Department of Mechanical, Aerospace and Materials Engineering, Muroran Institute of Technology, Muroran, Japan.

[e] Institute of Space and Astronautical Science, Japan Aerospace Exploration Agency, Sagamihara, Japan.

[f] Department of Geophysics, Tohoku University, Sendai, Japan.

Published online: 12 Sep 2013.

To cite this article: Jun Koyanagi, Akihito Watanabe, Nobuyoshi Kawabata, Tsuyoshi Ozaki, Ken Higuchi, Kosei Ishimura & Yasumasa Kasaba (2014) Long-term durability of tri-axial woven CFRP tube structure extended along the spin axis of spinning platforms for the SCOPE mission, Advanced Composite Materials, 23:2, 115-128, DOI: 10.1080/09243046.2013.835921

To link to this article: http://dx.doi.org/10.1080/09243046.2013.835921

Advanced Composite Materials, 2014
Vol. 23, No. 2, 115–128, http://dx.doi.org/10.1080/09243046.2013.835921

Long-term durability of tri-axial woven CFRP tube structure extended along the spin axis of spinning platforms for the SCOPE mission

Jun Koyanagi[a]*, Akihito Watanabe[b], Nobuyoshi Kawabata[b], Tsuyoshi Ozaki[c], Ken Higuchi[d], Kosei Ishimura[e] and Yasumasa Kasaba[f]

[a]*Department of Materials Science and Technology, Tokyo University of Science, Tokyo, Japan;* [b]*Sakase Adtech Co. Ltd., Fukui, Japan;* [c]*Composites Research and Development, Co. Ltd., Yokohama, Japan;* [d]*Department of Mechanical, Aerospace and Materials Engineering, Muroran Institute of Technology, Muroran, Japan;* [e]*Institute of Space and Astronautical Science, Japan Aerospace Exploration Agency, Sagamihara, Japan;* [f]*Department of Geophysics, Tohoku University, Sendai, Japan*

(*Received 10 June 2013; accepted 15 August 2013*)

This study investigates the strength and long-term durability of a spin-axis extensible rigid antenna element, made of tri-axial woven carbon fiber-reinforced polymer (CFRP), for a spinning spacecraft. Due to a slight deviation between the spin axis and antenna-extended axis with the spin, the antenna is subjected to centrifugal body force; the centrifugal force enhances the antenna deflection. A relationship between centrifugal force and antenna deflection is derived from beam theory. As the apparent material modulus decreases with time, the deflection increases simultaneously. The time dependence of mechanical properties of the tri-axial woven CFRP is hence examined by a creep test. The time-dependent failure criterion of the antenna is then examined using a flexural durability test. Based on the beam theory and experimental results, we examine the long-term reliability of applying the tri-axial woven CFRP to extensible rigid antenna for the spinning spacecraft, especially for SCOPE mission; it is verified that the current design tolerance for the mission assures certain durability for long-term usage.

Keywords: tri-axial woven composite; CFRP; aerospace application; viscoelastic; beam theory

1. Introduction

Tri-axial woven composite material made of carbon fiber-reinforced polymer composite (CFRP) is light, thin, durable, stiff, and even flexible. These characteristics have received particular attentions during this decade.[1–9] One of the promising applications is the several types of rigid antennas extensible from the spacecraft, since its conductivity is enough in a wide frequency range.[10–12] In such cases, the CFRP antenna element is stored in the storage device before the launch, and extended to the outside on the orbit.

For monopole and dipole antennas or booms with straight and long shapes, its usual structure is a so-called storable extendible member (STEM).[10] Figure 1 shows an example, a single STEM antenna with the storage device, which was developed as the

*Corresponding author. Email: koyanagi@rs.tus.ac.jp

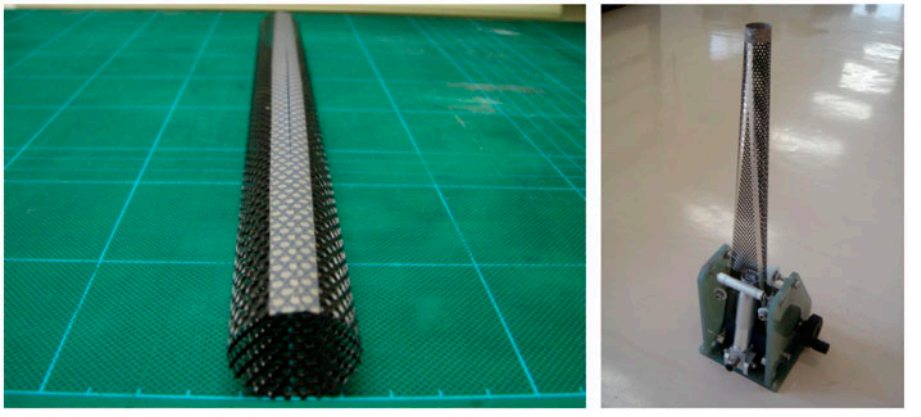

Figure 1. Single STEM made of tri-axial woven CFRP with the length of 5 m and the diameter of ~25 mm: (left) single STEM antenna element and (right) STEM antenna element attached to the storage device. The tip part of the element is closed by a small bolt. Its edges are protected by Teflon tape.

bread board model of monopole antenna with the length of 5 m and the diameter of ~25 mm for the Scale Coupling in Plasma Universe (SCOPE) mission planned by JAXA,[13] a formation flight mission for terrestrial magnetospheric studies by *in situ* multipoint and simultaneous observations of space plasmas surrounding the Earth. In this mission, tri-axial woven CFRP is used for a rigid antenna extended along the spin axis from a spinning satellite with a spin rate of ~20 rpm. When the antenna axis is completely extended on the spin axis, almost no load of the centrifugal force is applied to the antenna. However, there should remain some differences between the antenna location and spin axis. In such cases, the antenna is subjected to more or less eccentric spin motion.[14] This load adds deflection which increases the rotational radius, so that centrifugal force increases further. In order to achieve this design goal, straightness of the CFRP antenna element and the precise extension angle kept by the storage device are the key items. For the SCOPE mission, we already achieved such design and will be able to extend the rigid CFRP antenna with 5 m length along the spin axis in 20 rpm rotation.[11] In order to have sufficient stiffness requested for this spin-axis antenna, we will use bi-STEM antenna, in which two STEMs are duplicated (one overlapped on another). It is bounded by friction between each element, without direct mechanical fixation except for its tip.

The next problem is the long-term durability of the eccentric spinning antenna. The deformation of CFRP is time-dependent, even for the fiber-reinforced direction (time-independent fiber-properties governing direction),[15] because an apparent modulus of CFRP simply decreases with time. Assuming that the elastic deflection and centrifugal force are in equilibrium, the decrease of the modulus engenders an increase of deflection, which in turn demands a further increase of centrifugal force. In such process, the spin-induced deflection is enhanced over time, possibly exponentially, which eventually causes a time-dependent failure. It is the key issue for the long-term reliability of the spinning antenna, in order to set the design tolerance which can avoid the fatal failure during the operative period. Some knowledge of the time-dependent properties of the tri-axial woven CFRP material is indispensable. However, previous reports have mainly described them in static conditions [1–8]; note that Ref. 9 presented regarding its fatigue characteristics.

In this paper, we evaluate the long-term durability of a rigid tri-axial woven CFRP element, by the formulation of viscoelastic behavior determined by a creep test using a coupon specimen (Section 2) and the experimentally obtained flexural strength depending on applied-load history (Section 3). Based on them, we try to achieve the time-dependent failure prediction of the CFRP antenna and discuss the long-term reliability of tri-axial woven CFRP antenna with quantitative design tolerance of antenna lifetime (Section 4).

2. Creep test

2.1. Test condition

The viscoelastic property of a material is indispensable to discuss the long-term reliability of its structure. In our application, the applied load is similar to a creep load. Figure 2 shows the creep test specimen fabricated at Sakase Adtech Co., Ltd. The used fiber is 'T300' produced by Toray Co. Inc. The matrix is common epoxy resin. It was cured at 180 °C for 1 h. The gage length is 100 mm, its width is 25 mm, and its thickness is 0.14 mm. The specimen direction is transverse, i.e. the three axial directions are 30°, 90°, and 150°, which are the same directions as the application of this material to a satellite extensible antenna element. A static tensile failure load of this specimen is 494 N and the failure strain is 1.12% on average.

For the creep test, a constant load was applied to the specimen at room temperature (23 °C). The maximum creep time was 167 h (=10,000 min). We measured the displacement within the gage length by an extensometer attached with the cross heads of testing machine.

2.2. Test results and formulation

Figure 3 shows the test results. Upper panel shows the cases of high applied load (0.8–0.925 times of static failure load) that can engender ultimate creep rupture. Lower panel shows the low applied-load cases (0.1–0.8 times of static failure load). Solid curves show experimental results. Dotted curves show the predicted strain as a function of time defined as follows: First, the reinforcement is not aligned in the tensile direction, so that viscoelastic behavior of this composite is rather similar to that of matrix resin. To express the relaxation modulus of epoxy resin, we use the following generalized Voigt model equation as in conventional studies.[15–18]

$$E(t) = \frac{1}{J_0\{1 + (t/T_0)^n\}} \tag{1}$$

Here, $E(t)$ represents the time-dependent relaxation modulus, J_0 denotes static compliance, t stands for time, T_0 is specific relaxation time, and n is a power law exponent. In the present study, we adopt this equation to composite viscoelastic deformation. For the present study, we assume that the material follows Equation (1) and determine $n = 0.3$ and $T_0 = 50{,}000$ h by fitting.

Comparisons between experimental and predicted strains are presented in Figure 3. The predicted and experimentally obtained strains have some deviations depending on the load ratio. When the applied strain is high, the prediction underestimates the time-dependent strain, which is true mainly because of a non-linearity of viscoelastic

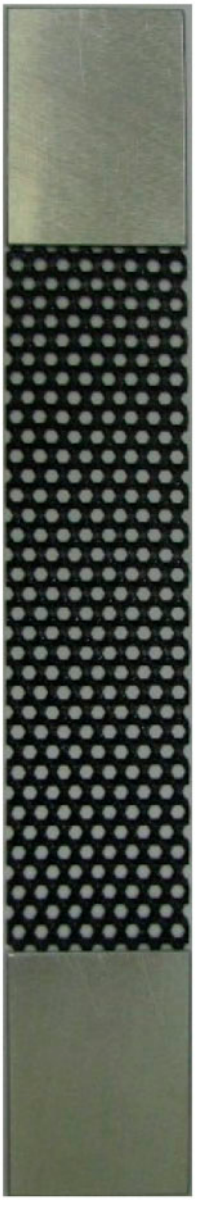

Figure 2. Tri-axial woven composite specimen used for creep tests. Size is $100 \times 25 \times 0.14$ mm. Fiber directions are 30°, 90°, and 150°. Top and bottom parts are strengthened by aluminum tabs for a firm grip.

deformation at high stress. The predictions are therefore aggressive in this case. In contrast, when the applied load is low, the predictions overestimate or are close values to experimentally obtained results, so that the predictions are conservative. The formulation might be too simple to apply for tri-axial CFRP. This aspect is important for our future work. Indeed, unit cell simulation considering geometrical change should be done for precise strain prediction.

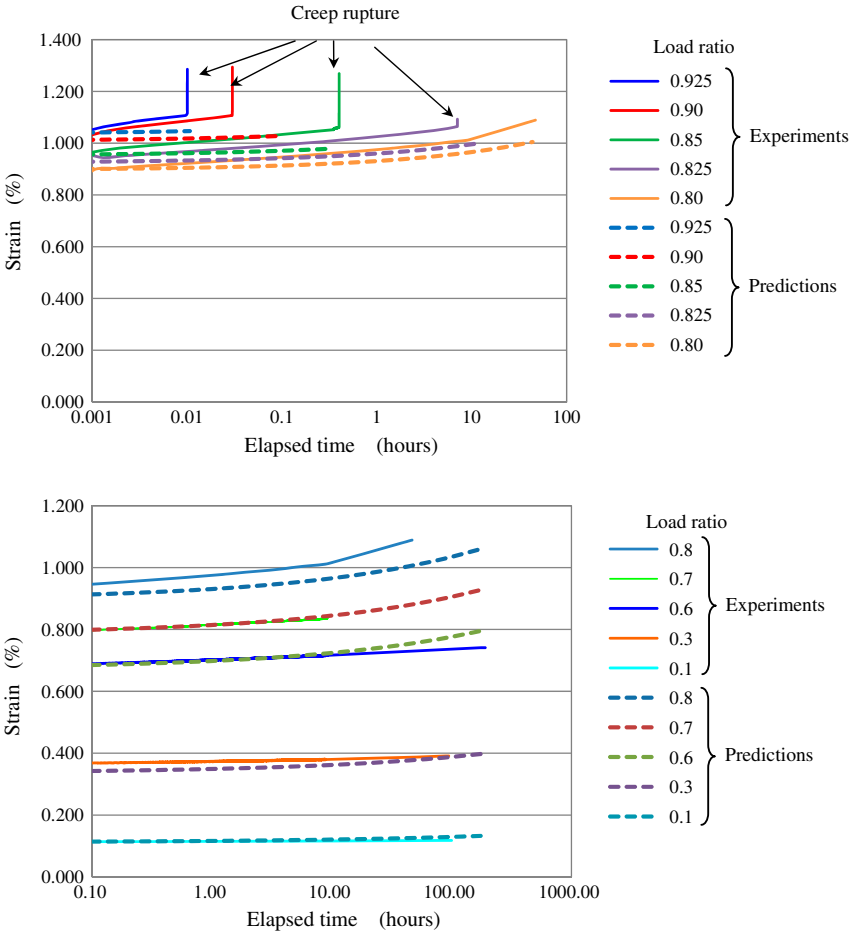

Figure 3. Strain with elapsed time under creep loads of 0.925–0.1 times of static failure load. Solid curves are experimentally obtained results. Dotted curves are predictions: (upper) high applied-load cases (0.8–0.925) and (lower) low applied-load cases (0.1–0.8).

3. Flexural durability test

3.1. Specimen

Next, we investigate the time dependence of flexural strength. Figure 4 presents a specimen of the bi-STEM antenna element stored in the storage device, with the definition of x–y–z coordinates. Table 1 shows the specimen properties obtained experimentally with the assumption that it is approximately a homogeneous solid column. Open cross sections are located at contrary phases on the x-axis. A flexural load is applied to the y-direction because the flexural strength in the y-direction is weaker than that in the $+x$ or $-x$ direction found in the results of static flexural tests, which are contributed by the open section shown in the bottom right panel of Figure 4.

3.2. Experimental procedure

In order to discuss the long-term durability of a material, the time-dependent failure criterion of the material must be clarified. The time-dependent material strength is

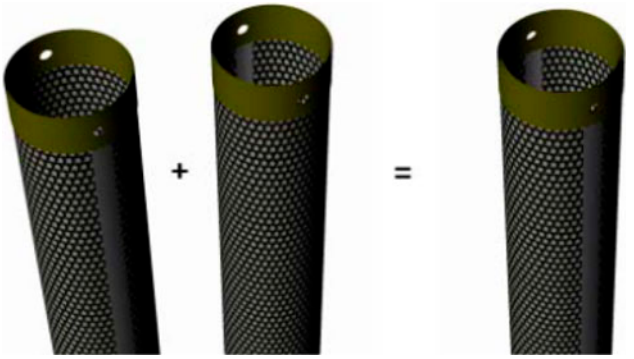

(a)

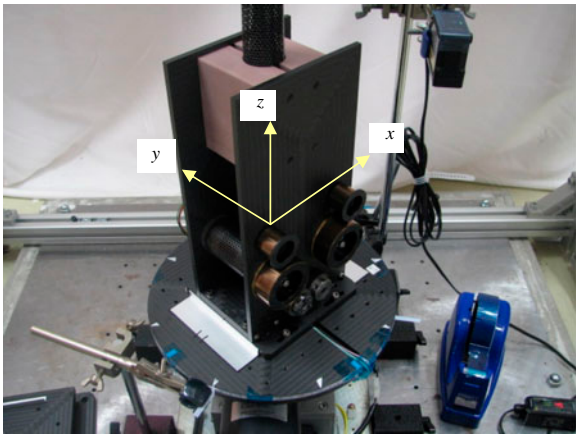

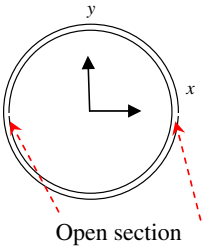

(b)

Figure 4. Double-wrapped STEM specimen (bi-STEM): (a) schematic of double-wrapped STEM what we call bi-STEM and (b) bi-STEM specimen attached within reel device and definition of *x*–*y*–*z* coordinates. Flexural test is performed in the *y*-direction, which shows the weakest static flexural strength.

Table 1. Material properties of the tested specimen.

Property	Symbol	Value	Unit
Density	ρ	42.5	kg/m^3
Cross-sectional area	A	5.18E−04	m^2
Initial compliance	J_0	1.28E−09	Pa
Moment of inertial of area	I	2.13E−08	m^4
Rotational speed	ω	2.094333	rad/s
Length	l	5.0	m

usually dominated by the applied-load history. If the applied stress rate differs, the strength would also be different.[19–21] The experimental configuration is presented in Figure 5. The specimen is set diagonally and is supported by a storage device part at

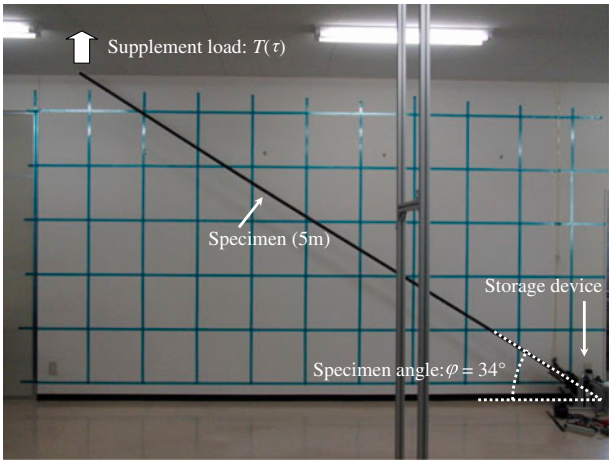

Figure 5. Flexural test configuration. Main load is made by gravity and a supplement load T is applied at the top of specimen to upper direction. Without this supplement load, the specimen fails from gravitational body force alone. The supplement load T decreases with the step of 9.8×10^{-3} N by every corresponding elapsed time.

the root. A supplemental load is applied to the top of the specimen via pin-tensile by a tensioned string. The applied moment is controlled by fixed gravitational forces and variable supplemental load. The initial value of the supplemental load, $T(0)$, is half of the gravitational force by the specimen weight. In this configuration, the supplemental load $T(\tau)$ is the function of time, i.e. decreased monotonically with the step of 9.8×10^{-3} N. The maximum moment, which occurs at the support at the root by the storage device, can be written as the following equation:

$$M_{\max}(\tau) = \frac{1}{2} A\rho g \cos\varphi \cdot l^2 - T(\tau) \cos\varphi \cdot l \tag{2}$$

$$T(\tau) = \frac{1}{2} A\rho g l - gc\tau \tag{3}$$

Here, A is the cross-sectional area of the specimen, ρ represents density, g stands for gravity acceleration, φ (=34°) is the angle between specimen axis to horizon, l denotes the specimen length, T is the supplemental load, τ is time (second), and c is the supplemental weight decreasing rate. The present study adopts $c = 10^{-4}$, 10^{-5}, 10^{-6}, and 10^{-7} kg/s. Finally, in those equations, gc consists of a constant mass rate (c) multiplied by gravity acceleration (g) and the present study actually uses a *round down function* for the value of $1000 \times c\tau$. In fact, $T(\tau)$ is controlled by many 1 g coins via a pulley with stringer. In other words, $T(\tau)$ decreases 9.8×10^{-3} N by each corresponding time interval. The experiment was conducted at room temperature (approximately 20 °C).

3.3. *Experimental results*

During a decreasing supplement load, the specimen fails as shown in Figure 6. The failure point is indicated in Figure 6(a). Its failure manner is closed up in Figure 6(b).

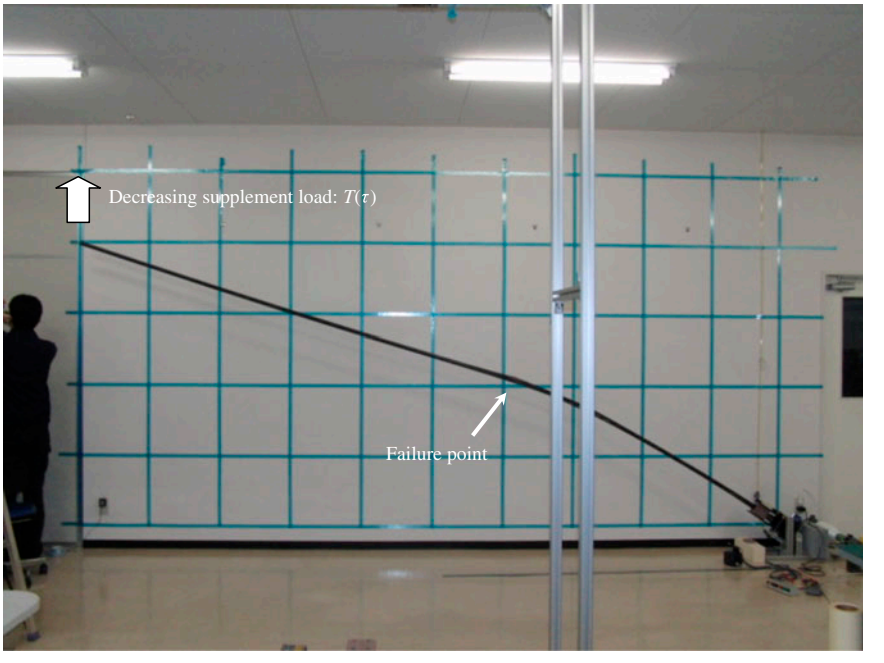

(a) Failure specimen

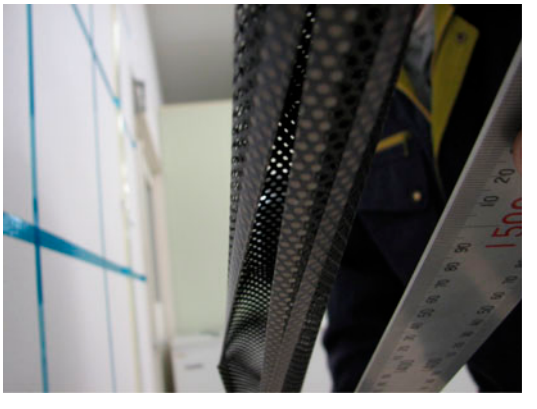

(b) Close-up photograph at failure part

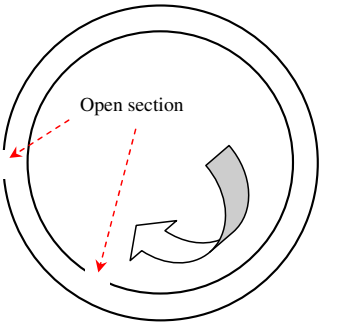

(c) Schematic of slipping of each STEM

Figure 6. Flexural failure behavior of bi-STEM element: (a) whole view, (b) close-up of the failure part, and (c) partial schematic of failure mechanism. The failure position and mechanism for all specimens are similar. Each STEM sliped beyond the friction, and large deformation occurred when both open sections were in same side.

Figure 6(c) schematically shows the failure behavior at that part. In the experiment of our bi-STEM structure, the failure occurs by slipping of each STEM element, and both open sections are approaching to the same side, i.e. each element rotates in individual direction in order to make the whole potential energy minimum. For all tests, this failure behavior and the failure point are common. Figure 7 summarizes the relationship between the time-to-failure and maximum flexural moment at that time. Unexpectedly, the maximum flexural moment is independent of the time-to-failure, which means that

the failure criterion is time-independent. The failure moment is the same level, nevertheless the time-to-failure ranging to a thousand times, is not general. Even the tensile strength of unidirectional CFRP, which is considered significantly stolid with time-to-failure, varies with 1000 time's change of that.[16]

The present study interprets this experimentally obtained result as follows: careful observation of failure behavior in Figure 6 shows that the flexural failure was triggered by the slipping of each STEM, and then large deformation followed involving local damage. The failure time is therefore governed by the slipping. The friction might be time-independent, as was assumed in several conventional articles.[15,17] This assumption can recognize the flexural failure criterion of this material as time-independent. The factor dominating the slippage is possibly the whole flexural moment. This study assumes that when the maximum flexural moment becomes not less than 1.5 Nm, the specimen fails. This criterion is applicable only for our bi-STEM specimen in which both STEM elements are frictionally fixed, without direct mechanical connections. If the failure criterion is time-dependent, then a time-dependent failure law should be considered based on Equation (2), but the present study does not need to do that.

4. Time-dependent failure prediction

4.1. Deflection induced by centrifugal force

In this section, we evaluate the deflection-induced centrifugal force based on linear beam theory. Figure 8 shows the geometrical definition of the off-set dimension δ and axis tilt θ. Note that δ and θ are small enough and the infinitesimal deformation is assumable. For the spin-axis antenna, a distributed load by of the centrifugal force is applied as the function of deflection (rotational radius). The following equation should be satisfied between the deflection function and centrifugal force. (In this study, we assume that directions δ and θ are the y-direction of Figure 4 for postulating the worst case.)

$$\frac{\partial^4 U(x,t)}{\partial x^4} = \frac{1}{E(t)I}\rho A U(x,t)\omega^2 \quad \beta(t) = \sqrt[4]{\frac{\rho A\omega^2}{E(t)I}}$$
$$\frac{\partial^4 U(x,t)}{\partial x^4} = \beta(t)^4 U(x,t) \tag{4}$$

Here, U represents the deflection, x is the position, $E(t)$ is related to Equation (1), ρ stands for the material density, A is the material cross-sectional area, ω is the spin rate, and I denotes the moment of inertia of area. The material properties, regarded as

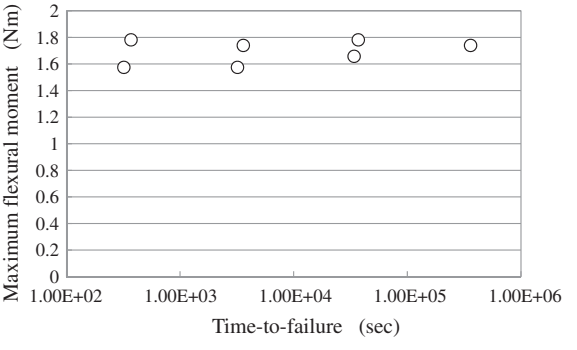

Figure 7. The relationship between maximum flexural moment and time-to-failure.

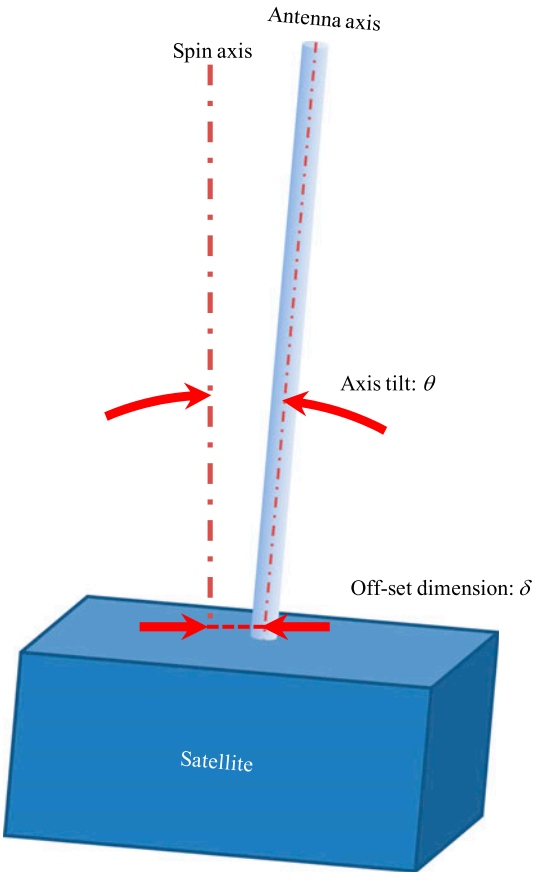

Figure 8. Definition of off-set dimension δ and axis tilt θ. δ is distance from spin axis to attachment part of antenna axis. θ is angle between spin axis and antenna axis.

homogeneous solid column, are listed also in Table 1. For the simplification, we ignore the effects of open sections of the specimen. The general solution of Equation (4) is shown as:

$$U(x,t) = C_1 \cos\beta(t)x + C_2 \sin\beta(t)x + C_3 \cosh\beta(t)x + C_4 \sinh\beta(t)x \tag{5}$$

The following boundary conditions are used to derive the values of C_1–C_4.

$$\begin{aligned} U(0,0) &= \delta \\ U'(0,0) &= \theta \\ U''(l,0) &= 0 \\ U'''(l,0) &= 0 \end{aligned} \tag{6}$$

Consequently, maximum flexural moment occurs at the antenna joint part. The value is written as shown below.

$$M_{\max}(t) = \frac{\theta\{\cos\beta(t)l \sinh\beta(t)l - \sin\beta(t)l \cosh\beta(t)l\} - \delta\beta(t)\sin\beta(t)l \sinh\beta(t)l}{1 + \cos\beta(t)l \cosh\beta(t)l}\beta(t)E(t)I \tag{7}$$

Figure 9 shows the predicted deflections of the antenna element with the assumption of $\delta = 0.05$ m and $\theta = 0.02$ rad, which are the tolerance values in the design specifications set in the SCOPE mission study. *X*–axis is the position from the root. *Y*–axis is the amount of deflection. The predicted deflections at $t = 0$ (initial), 82 h, 2600 h (∼108 days), and 42,000 h (∼4.8 years) are shown. Figure 10 presents the time evolution of the predicted deflection at the antenna top part (maximum deflection) and maximum flexural moment.

In both figures, the deflection and maximum moment increase with time. Time-dependent failure occurs when the time-dependent failure criterion is satisfied. [15,16,18,19] As described in Section 3, for this specimen the failure criterion does not depend on time; the reliability is identifiable using only maximum flexural moment as a function of time. In Figure 10, after approximately 5 years elapse, the maximum flexural moment is still around 0.3 Nm, which is much less than the expected failure criteria, 1.5 Nm. Keeping the original set tolerance values, it can be expected the long-term reliability of spinning antenna would sufficiently be guaranteed.

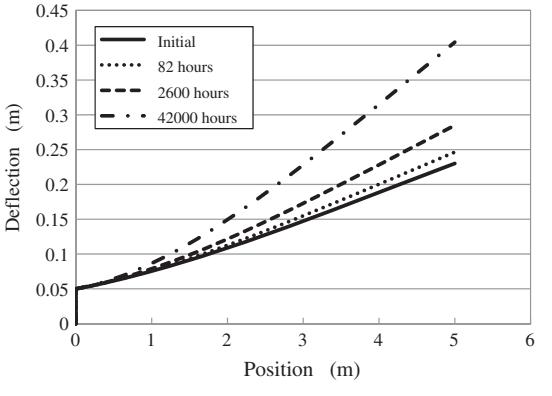

Figure 9. The predicted deflections as a function of time (assuming $\delta = 0.05$ m and $\theta = 0.02$ rad).

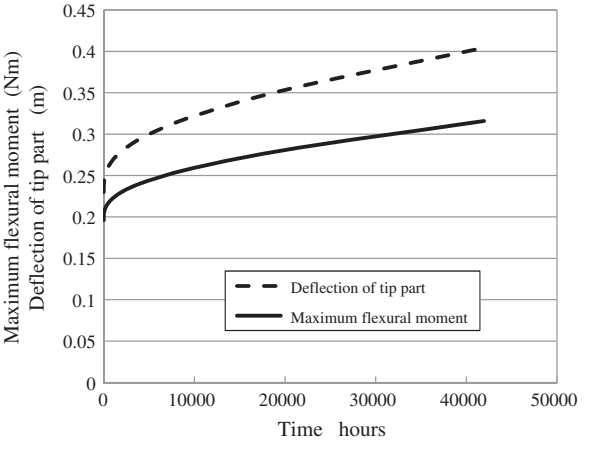

Figure 10. Predicted deflections of tip part and maximum flexural moment as a function of time (assuming $\delta = 0.05$ m and $\theta = 0.02$ rad).

4.2. Discussion

There are still several assumed and/or unknown factors in the durability assessment above. These effects should be organized and discussed.

First, the approximation of viscoelastic behavior does not exactly agree with the experiments as shown in Figure 3. In order to address this problem, we must produce a model from meso-scopic perspective and to consider meso- and micro-scale strain localization and its time dependence. Especially at the crimp part (fiber-tow intersecting part), remarkable strain localization can occur. No article in the relevant literature has described an experimental investigation of the meso-scale strain localization using for example digital image correlation (DIC) technique [22] and so on. Reliable modeling is a subsequent study to be done in the near future. Regarding limitations of this study, the approximations underestimate experimentally obtained results at low applied stress so that the prediction is sufficiently safe and useful.

Secondly, the time dependence of flexural strength of bi-STEM has not been supported by theoretical evidence. In Section 3, our experiment indicates that the failure criterion is time-independent but a prediction beyond experimental time range, what we call extrapolation, must be explained by valid logic. For this issue, modeling each STEM individually would be effective, which requires knowledge of the realistic viscoelastic behavior of tri-axial woven CFRP itself also. This problem is expected to be clarified before the satellite launches.

A third factor is that large deformation is not considered in the deflection calculation. When considering the large deformation, the specimen length (l) becomes shorter, which causes the amount of centrifugal force, which is equivalent to the maximum flexural moment, to decrease. Consequently, the present prediction produces a more conservative result than the actual one.

As a fourth factor, we do not consider the history-dependent apparent elastic modulus, and simply use Equation (1). Generally, a viscoelastic constitutive equation should be written in a form of convolution integral that can consider load or strain history.[15] When a load history increases monotonically, the apparent elastic modulus is always greater than that solely given by Equation (1). Therefore, the fourth factor also serves to produce a conservative prediction.

The fifth and last concern is temperature dependence. Usually, an elevated temperature accelerates the time progress.[16] The present prediction postulates room temperature; if the room temperature is higher than that in a space environment, the prediction becomes conservative. For the SCOPE mission study, we confirmed in rough thermal model analysis that the temperature of this antenna element becomes not so high. However, it should also be more careful for wider applications.

We list the five uncertainties against reliability prediction described as a result of this study. The second one, scarcity of theoretical evidence of time-independent flexural failure criterion of bi-STEM specimen, must be studied in the near future; the other factors serve to produce conservative predictions.

5. Conclusion

This paper evaluated the long-term reliability of a tri-axial woven CFRP element which will be utilized as the rigid antenna extended along the spacecraft spin-axis with fast spin rotation, $\sim$20 rpm. Creep behavior of tri-axial woven CFRP and time dependence of flexural failure of bi-STEM antenna were experimentally investigated. A relationship of the deflection induced by centrifugal force was derived from the beam theory. Based

on the results, we estimated maximum flexural moment and deflection that increase with time. We then discussed the reliability of the antenna application considering the tolerance gap of the antenna axis and satellite spin axis given by the design configuration of the SCOPE mission. The current design was found to be sufficiently conservative in terms of long-term durability.

Acknowledgments

We express our thanks to Dr Y. Saito and all SCOPE mission study members in the Next Generation Magnetospheric Mission Working Group. We acknowledge the commitment of Dr K. Ishizaka, Dr H. Kojima, and Dr A Kumamoto for this development as a part of Plasma Wave Investigation team.

References

[1] Fujita A, Hamada H, Maekawa Z. Tensile properties of carbon fiber triaxial woven fabric composites. J. Compos. Mater. 1993;27:1428–1442.
[2] Zhao Q, Hoa SV, Moudrik R. Finite element modeling of a membrane sector of an art EM reflector. J. Compos. Mater. 2005;39:581–600.
[3] Xu D, Gaesan R, Hoa SV. Buckling analysis of tri-axial woven fabric composite structures. Part I: non-linear finite element formulation. Compos. Struct. 2005;67:37–55.
[4] Xu D, Ganesan R, Hoa SV. Buckling analysis of tri-axial woven fabric composite structures subjected to bi-axial loading. Compos. Struct. 2007;78:140–152.
[5] Zhao Q, Hoa SV. Triaxial woven fabric (TWF) composites with open holes (Part I): finite element models for analysis. J. Compos. Mater. 2003;37:763–789.
[6] Aoki T, Yoshida K. Mechanical and thermal behavior of triaxially-woven carbon/epoxy fabric composite. In: Proceedings of the 47th AIAA/ASME/ASCE/AHS/ASC Structures, Structural Dynamics and Materials Conference, AIAA 2006-1688; 2006; Newport, Rhode Island.
[7] Aoki T, Yoshida K, Watanabe A. Feasibility study of triaxially-woven fabric composite for deployable structures. In: Proceedings of the 48th AIAA/ASME/ASCE/AHS/ASC Structures, Structural Dynamics and Materials Conference, AIAA 2007-1811; 2007; Honolulu, Hawaii.
[8] Aoki T, Furuya H, Ishimura K, Miyazaki Y, Senda K, Tsunoda H, Higuchi K, Ishizawa J, Kishimoto N, Sakai R, Watanabe A, Watanabe K. On-orbit verification of space inflatable structures. Trans. JSASS Space Technol. Jpn. 2009;7:Tc1–Tc5.
[9] Aoki T, Kosugi Y, Watanabe A. Fatigue characteristic and damage accumulation mechanism of triaxially-woven fabric composite. In: Proceedings of the 52nd AIAA/ASME/ASCE/AHS/ASC Structures, Structural Dynamics and Materials Conference, AIAA 2011-1993; 2011; Denver, Colorado.
[10] Higuchi K, Watanabe K, Watanabe A, Tsunoda H, Yamakawa H. Design and evaluation of an ultra-light extendible mast as an inflatable structure. In: Proceedings of the 47th AIAA/ASME/ASCE/AHS/ASC Structures, Structural Dynamics and Materials Conference, AIAA 2006-1809; 2006; Newport, Rhode Island.
[11] Kasaba Y, Kumamoto A, Ishisaka K, Kojima H, Higuchi K, Watanabe A, Watanabe K. Development of stiff and extensible electromagnetic sensors for space missions. Adv. Geosci. 2010;21:447–459.
[12] Higuchi K, Ogi Y, Watanabe K, Watanabe A. Verification of practical use of an inflatable structure in space. Trans. JSASS Space Technol. Jpn. 2009;7:Tc7–Tc11.
[13] Fujimoto M, Tsuda Y, Saito Y, Shinohara I, Takashima T, Matsuoka A, Kojima H, Kasaba Y. The SCOPE mission. AIP Conf. Proc. Future Perspect. Space Plasma Part. Instrum. Int. Collab. Tokyo (Japan). 2009;1144:29–35.
[14] Ogi Y, Higuchi K, Ishimura K. Effect of attachment errors of flexible appendages on the spin axis of a rigid body. Trans. JSASS Space Technol. Jpn. 2012;10:Tc7–Tc12.
[15] Koyanagi J. Comparison of a viscoelastic frictional interface theory with a kinetic crack growth theory in unidirectional composites. Compos. Sci. Technol. 2009;69:2158–2162.
[16] Koyanagi J, Nakada M, Miyano Y. Tensile strength at elevated temperature and its applicability as an accelerated testing methodology for unidirectional composites. Mech. Time-Depend. Mater. 2012;16:19–30.

[17] Koyanagi J, Yoshimura A, Kawada H, Aoki Y. A numerical simulation of time-dependent interface failure under shear and compressive loads in single-fiber composite. Appl. Compos. Mater. 2010;17:31–41.
[18] Koyanagi J, Kiyota G, Kamiya T, Kawada H. Prediction of creep rupture in unidirectional composite (creep rupture model with interfacial debonding around broken fibers). Adv. Compos. Mater. 2004;13:199–213.
[19] Christensen RM. An evaluation of linear cumulative damage (Miner's law) using kinetic crack growth theory. Mech. Time-Depend. Mater. 2002;6:363–377.
[20] Christensen RM, Miyano Y. Deterministic and probabilistic lifetimes from kinetic crack growth-generalized forms. Int. J. Fract. 2007;143:35–39.
[21] Christensen RM, Miyano Y. Stress intensity controlled kinetic crack growth and stress history dependent life prediction with statistical variability. Int. J. Fract. 2006;137:77–87.
[22] Yoneyama S, Murasawa G. Digital image correlation, experimental mechanics. In: Freire JF, editor. Eolss; 2009. Available from: http://www.eolss.net/Sample-Chapters/C05/E6-194-04.pdf